HERON is jointly edited by:
STEVIN-LABORATORY of the department of Civil Engineering, Delft University of Technology, Delft, The Netherlands
and
INSTITUTE TNO for Building Materials and Building Structures, Rijswijk (ZH), The Netherlands.
HERON contains contributions based mainly on research work performed in these laboratories on strength of materials, structures and materials science.

ISSN 0046-7316

Secretary:
G. J. van Alphen
Stevinweg 1
P.O. Box 5048
2600 GA Delft, The Netherlands
Tel. 0031-15-785919
Telex 38070 BITHD

HERON vol. 30 1985 no. 4

Contents

STEEL COLUMN AND FRAME STABILITY ANALYSIS USING FINITE ELEMENT TECHNIQUES

R. J. van Foeken
H. H. Snijder
TNO Institute for Building Materials and Structures, Rijswijk, The Netherlands

YIELD SURFACE FOR BENDING MOMENT, SHEAR FORCE AND NORMAL FORCE

J. M. M. Out
Koninklijke/Shell Exploratie en Productie Laboratorium,
Rijswijk, The Netherlands

Abstract. Steel column and frame stability analysis using finite element techniques

The facilities for analysing steel columns and frames at room temperature and under fire conditions of the general purpose finite element program DIANA, are described in this paper. These facilities include among other elements a beam-column element, means to describe geometrical and material non-linear behaviour and several iteration procedures to solve non-linear beam-column problems. Use of these facilities is illustrated by several examples of beam-columns and frames. These examples clearly show that finite element techniques are of great help in steel column and frame stability research. Use of finite element techniques leads to a better understanding of structural behaviour and helps to attain better design rules.

Keywords: Steel, column, frame, stability, fire, design rules, beam-column, finite element method.

Steel column and frame stability analysis using finite element techniques

1 Introduction

To achieve a better understanding of structural behaviour the finite element method has been used more and more in the last twenty years. In a research and development environment advanced non-linear finite element techniques can be successfully applied to verify design rules presented by different codes. Also, complicated structures can be analysed with the finite element method, which cannot be checked using design rules or which cannot be experimentally investigated because of their sizes or boundary conditions. Very often structural behaviour is highly non-linear. Therefore, an appropriate constitutive relation has to be used when analysing structures with the finite element method.

At the research institute IBBC-TNO the general purpose finite element program DIANA has been developed. In this paper, only the beam-column element is extensively discussed. In DIANA, it is possible to take material and geometrical non-linear behaviour into account. The constitutive relation described in this paper is based on the classical plasticity theory in which the material properties can vary with temperature. This constitutive relation can be used together with geometrical non-linearity. In the next sections, the constitutive relation and geometrical non-linearity are described for the beam-column element. Some finite element aspects and some iteration procedures which are very effective for load controlled buckling problems, are briefly discussed. The presented theory is used to analyse beam-columns and frames at room temperature and under fire conditions.

2 Beam-column element, describing geometrical and material non-linear behaviour

2.1 *Theoretical formulation of the beam-column element*

To determine the deformation behaviour of steel frames, a beam-column element is defined based on the displacement finite element method.

In finite element analyses the structure is idealized as an assemblage of discrete finite elements with the elements being interconnected at nodal points on the element boundaries. The displacements within each element are assumed to be a function of the nodal displacements. The two-dimensional beam-column element has two nodes at the ends of the element with three degrees of freedom at each node: two translations and one rotation. For the in-plane displacement field within the element a cubic interpolation function is used. The axial displacement field is based on a parabolic interpolation function. For the parabolic function three nodal displacements are necessary. There-

fore, an additional internal node in the middle of the element with a degree of freedom, u_k, in the axial direction is assumed. This extra degree of freedom is condensed out of the element stiffness matrix and load vector at the element level. So externally only 6 degrees of freedom are present, see Fig. 1. The displacement function can be split into

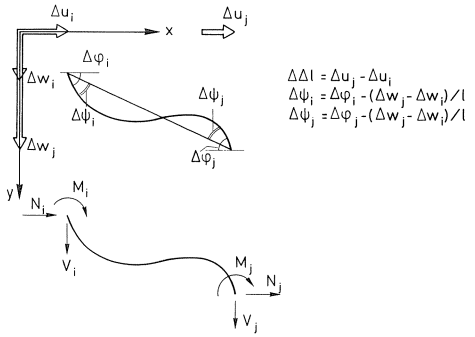

Fig. 1. Displacements and member end-forces for the beam-column element [4].

rigid displacements which do not change the stresses and displacements which lead to deformation of the element. These latter displacements are called the generalized displacements. The displacements along the element axis are described by equations (1) and (2) for the displacement perpendicular to the axis $w(x)$ and the displacement in the direction of the axis $u(x)$ respectively:

$$w(x) = \frac{x(l-x)^2}{l^2}\psi_i - \frac{x^2(l-x)}{l^2}\psi_j \tag{1}$$

$$u(x) = \frac{x}{l}\Delta l + \frac{4x(l-x)}{l^2}u_k \tag{2}$$

with x the local coordinate along the element axis. In the beam-column element shear deformation is not taken into account and the normal to the neutral axis remains straight during deformation. Therefore, using beam-column elements requires continuity of dw/dx on the element boundaries at the nodes.

Along the axis of the beam-column element an average strain $\varepsilon_g = du/dx$ and a curvature $\varkappa = -d^2w/dx^2$ are considered. The strain distribution over the section is determined by the relation:

$$\varepsilon = \frac{du}{dx} - y\frac{d^2w}{dx^2} \tag{3}$$

When the element axis coincides with the centroidal axis, the average strain at the element axis, ε_g, is equal to the strain at the centroidal axis, $\bar{\varepsilon}_g$. The centroidal axis is determined by the distribution of the stiffness over the cross-section; see Fig. 2. When these axes do not coincide, such as in non-linear problems, a shift of the centroidal axis

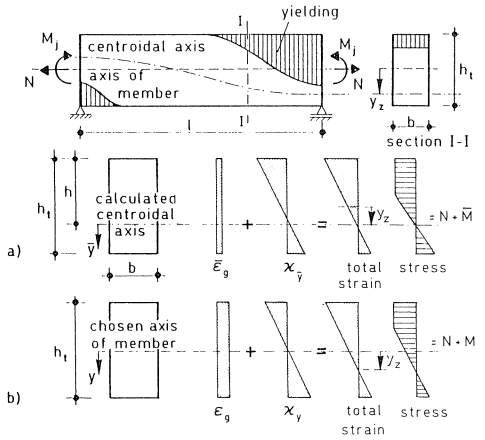

Fig. 2. Definition of average strain, curvature and centroidal axis.

from the element axis has to be taken into account. By using a parabolic interpolation function for the axial displacement field, this shift can be described. It follows from Fig. 2 that $\bar{\varepsilon}_g = \varepsilon_g + y_z \varkappa$.

To determine the relation between the external loads and the deformation field of the beam-column element, the principle of virtual work which describes equilibrium between internal and external forces is used within a total Lagrangian description [1,4]. This relation leads to a stiffness matrix which is derived in Appendix A.

In order to make numerical integration over the element possible, the element is divided in sections and each section in several layers. At the top and bottom of each layer an integration point is present. At each integration point a uni-axial strain is calculated from the displacement field. From this strain stresses and stiffnesses can be calculated using the constitutive relation, given in section 2.3. Integration of the layers leads to an internal moment and normal force and the stiffnesses for each section.

Between the integration points of each layer a linear interpolation for stresses and stiffnesses is adopted; see Fig. 3. The contribution of the stress and stiffness at the top of the layer to the moment, the normal force and the stiffnesses of a section is determined, assuming a triangle with the stress and stiffness at the bottom of the layer being zero. For the bottom of the layer the same procedure is used, see also Fig. 3. Integration of the section forces and stiffnesses using the Simpson rule leads to a stiffness matrix and internal forces at nodes of the element.

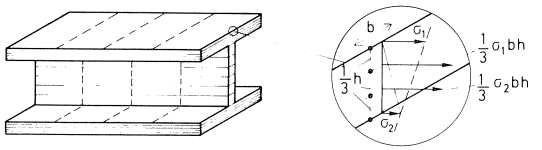

Fig. 3. Element divided in sections and layers.

2.2 *Geometrical non-linearity*

In the previous paragraph it has been implicitly assumed that both displacements and strains in the structure are small. In practical terms this means that the geometry of the elements remains basically unchanged during the loading process and that first order infinitesimally small linear strain approximations can be used.

When the displacements are large, the previous assumptions fail even when the strains remain small and the material behaviour remains elastic. Now an accurate description of the deformations is needed and geometrical non-linearity has to be taken into account. This is the case when dealing with stability problems.

For the description of the deformation behaviour of the structure a total Lagrangian formulation is used, assuming large displacements but small strains. The strain distribution over the section as a function of the displacements is of the form:

$$\varepsilon = e + \eta = \frac{\mathrm{d}u}{\mathrm{d}x} - y\frac{d^2w}{\mathrm{d}x^2} + \tfrac{1}{2}\left(\frac{\mathrm{d}w}{\mathrm{d}x}\right)^2 \tag{4}$$

The non-linear contribution to the strain, $\eta = \frac{1}{2}(\mathrm{d}w/\mathrm{d}x)^2$, leads to an extra term in the incremental virtual work equation; compare equation (B.1) of Appendix B with equation (A.2) of Appendix A. The extra term in equation (B.1) leads to an initial stress matrix and an initial displacement matrix. The initial stress matrix accounts for the second order generalized deformations caused by the normal force and the initial displacement matrix is a correction for additional reactions caused by the normal force due to an inclination of the member. The element length, l, in equations (B.4) and (B.5) has to be updated at every load increment and during the loadstep at every iteration. In fact, a correction should also be applied to account for the change in length, $\Delta\Delta l$, of the member. When the member is subjected to bending moments the resulting deflection of the member causes its ends to move towards eachother. However, for most common structures this effect can be neglected, even in second order calculations [4].

2.3 *Non-linear material behaviour*

When the stresses are large, material non-linearity has to be taken into account for steel. For the beam-column element an elasto-plastic-creep material model is adopted, which is characterized by an initial yield criterion, a normality condition and a hardening rule. For steel the Von Mises yield function can be used as a criterion for yielding. Furthermore, the yield stress, Young's modulus and the thermal expansion can be modelled as a function of temperature. The material model used in the beam-column element can also be used with other element types which are available, such as plane-stress elements and shell elements, because the material model is a general three dimensional formulation [10] based on the classical plasticity theory.

In non-linear problems the loading is applied incrementally. At the end of each load increment an equilibrium state is reached by performing a number of iterations. Therefore, the constitutive relation has to be of an incremental form. See the next section for the iteration procedures.

Here, the case of a uni-axial stress state with the Von Mises yield criterion is considered. Let 0 and 1 refer to the beginning and end, respectively, of the loadstep. The total incremental strain can be expressed as the sum of the incremental elastic, plastic, creep and thermal strains:

$$\Delta\varepsilon = \Delta\varepsilon_e + \Delta\varepsilon_p + \Delta\varepsilon_c + \Delta\varepsilon_\Theta \tag{5}$$

The incremental thermal strain $\Delta\varepsilon_\Theta$ depends on the temperature increment and thermal expansion only. The incremental creep strain $\Delta\varepsilon_c$ can be specified by a creep law. For steel, creep is only relevant at high temperatures. The incremental elastic strain $\Delta\varepsilon_e$ is reversible and is related to the incremental stress by Hooke's law:

$$\Delta\sigma = E^1\Delta\varepsilon_e + \Delta E\varepsilon_e^0 \tag{6}$$

In equation (6) the second term on the right hand side is due to a change of Young's modulus with temperature. Young's modulus is evaluated for the temperature at the end of the increment. To determine whether the status of an integration point is elastic or plastic the Von Mises yield criterion is used. For a uni-axial stress state the Von Mises yield function including strain hardening can be formulated as follows:

$$f(\sigma, \varepsilon_p, \Theta) = |\sigma| - \sigma_y(\varepsilon_p, \Theta^1) \tag{7}$$

The yield function f depends on the plastic strain, the temperature at the end of the increment and the stress. When $f<0$ the status of the integration point is elastic and for $f\geqslant 0$ this status is plastic.

The incremental elasto-plastic-creep relation for the uni-axial stress state is of the form:

$$\Delta\sigma = E^1(\Delta\varepsilon - \Delta\varepsilon_c - \Delta\varepsilon_\Theta) + \Delta E\varepsilon_e^0 - \frac{f(\sigma^e, \varepsilon_p^0, \Theta^1)E^1}{E^1 + H} \tag{8}$$

This relation is graphically explained in Fig. 4. The first two terms are due to the elastic behaviour and the third term is a correction for the plastic behaviour. The first term is represented by line AB in Fig. 4 and the second term in equation (8) is represented by

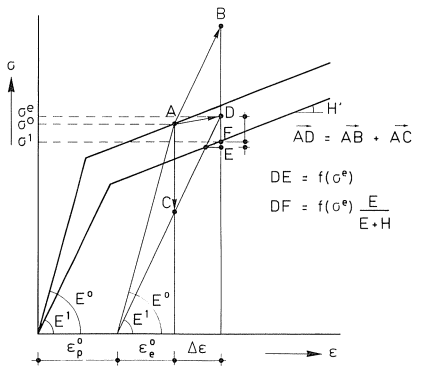

Fig. 4. Temperature dependent stress-strain relation with elastic unloading.

line AC in Fig. 4. Summation of AB and AC gives AD. The stress σ^e is the test stress to determine if an integration point is plastic or elastic. The test stress is determined by the relationship:

$$\sigma^e = \sigma^0 + E^1(\Delta\varepsilon - \Delta\varepsilon_c - \Delta\varepsilon_\Theta) + \Delta E\varepsilon_e^0 \tag{9}$$

The yield function value $f(\sigma^e, \varepsilon_p^0, \Theta^1)$ is represented by line DE. The third term in equation (8) is equal to the line DF. The hardening diagram can be constructed from a uni-axial stress-strain relation as shown in Fig. 5. Now the value of H can be determined.

The constitutive relation can also be combined with a tension stiffening relation for concrete under tension [12].

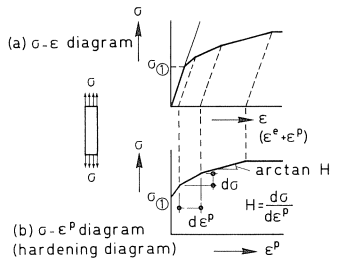

Fig. 5. The construction of the hardening diagram.

2.4 *Finite element aspects*

In general, a structure can undergo large displacements and the constitutive relation is non-linear, so that equation (B.1) cannot be solved directly by relating all variables to a previously calculated equilibrium state and by linearizing the equation. The solution of a non-linear problem can be achieved by iteration.

Substitution of the previously derived relations for the stiffness matrix, equation (A.8), the initial stress matrix, equation (B.4), the initial displacement matrix, equation (B.5) and the constitutive relation, equation (8) in equation (B.1) gives:

$$(K + K_\sigma^{NL} + K_L^{NL})\Delta v = \Delta P + \int_{V_0} \left(E^1(\Delta\varepsilon_c + \Delta\varepsilon_\Theta) - \Delta E\varepsilon_e^0 + \frac{f(\sigma^e, \varepsilon_p^0, \Theta^1)E^1}{E^1 + H} \right) dV \tag{10}$$

The variation of strains is related to the initial configuration, so the integration is carried out on the undeformed structure. The creep strain, the thermal strain, the change of the material properties with temperature and the plasticity part have been placed in the load vector, and the right side of equation (10) is now called the effective load vector. The effective load vector is only formed at the beginning of the load step. During the iteration process the differences between internal and external loads are determined which are applied as loads in the next iteration.

Several iteration procedures are available in DIANA [5], e.g. the Modified Newton-Raphson scheme in which the stiffness matrix is updated at the beginning of the load step and held constant during the iteration process, the Newton-Raphson scheme, in

which the stiffness matrix is updated at every iteration or the Quasi-Newton scheme as proposed by Crisfield or the scheme as proposed by Riks [17] and Wempner [28].

The method proposed by Riks and Wempner is very effective for load controlled snap-through and buckling problems, see Fig. 6. Limit points can be passed by help of

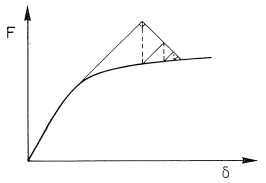

Fig. 6. Riks-Wempner iteration procedure.

an arc-length procedure. This method is used for the example of a sway frame as shown in the next chapter. However, for most examples the Newton-Raphson scheme is used.

The beam-column element described can also be used within DIANA in combination with other element types, e.g. solid-, plane-stress-, spring- and shell elements.

3 Applications at room temperature

The theory presented in the previous sections has been used to analyse columns, beams, beam-columns, non-sway frames and sway frames. A selection of examples is presented here. In this section attention is focussed on structures at room temperature.

3.1 *Centrally loaded pin-ended column*

The maximum strength of centrally loaded pin-ended steel columns is determined by two major different influences: residual stresses and geometrical imperfections. These influences have been examined thoroughly in the past. Research has lead to the introduction of multiple column curves. In Europe five different buckling curves (Fig. 7) are used by the ECCS [3,18]. These curves have been adopted in Eurocode No. 3 [8]. The maximum strength of the column of Fig. 8 can be calculated using curve b of Fig. 7. With $\bar{\lambda} = 1.28$ as slenderness parameter, the buckling stress $\sigma_k = 0.44\sigma_y$ is found. For Fe 360 with $\sigma_y = 240$ N/mm^2 we find $F = 269$ kN for the maximum strength.

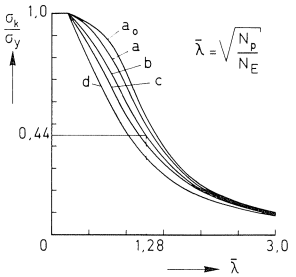

Fig. 7. European buckling curves [3, 18].

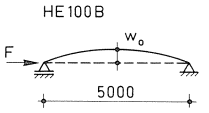

Fig. 8. Centrally loaded pin-ended steel column.

When analysing the in-plane behaviour of this centrally loaded pin-ended column using a finite element program taking account of geometrical and material non-linearity, geometrical imperfections and residual stresses have to be chosen. In [7,8] the imperfections of Fig. 9 are prescribed.

The computer analysis has been carried out using ten elements. Each element has been divided in five sections. For each section, 17 integration points have been chosen: 7 for the web and 5 for each flange. The total number of integration points is 85 per element.

The influence of the residual stresses in the web is small since the web does not contribute significantly to the flexural resistance [2] and this influence is neglected. The influence of the residual stresses in the flanges is taken into account by a modification of the stress-strain relation as given in Fig. 10. The modified stress-strain relation for the flanges can be determined by a calculation which simulates a stub-column test on a single flange, containing the residual stress pattern of Fig. 10. With the geometrical imperfection of Fig. 9 and the residual stresses of Fig. 10, line 1 in Fig. 11 is found as load-deflection curve. The computed maximum strength $F_1 = 292$ kN overestimates the maximum strength resulting from the ECCS buckling curves $F = 269$ kN by 8.5%.

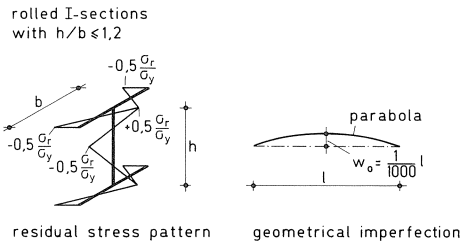

Fig. 9. Imperfections [7, 8].

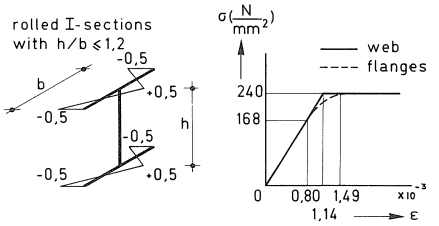

Fig. 10. Modelling of residual stresses.

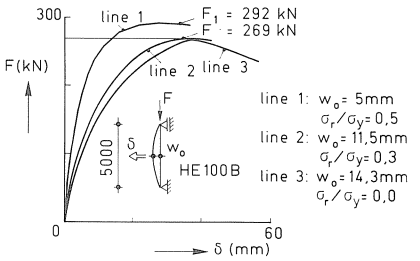

Fig. 11. Load-deflection curves of a centrally loaded pin-ended column.

A different approach to the column of Fig. 8 is: determine the amplitude of the parabolic imperfection w_0 so that the pin-ended centrally loaded column attains collapse at the maximum strength resulting from the ECCS buckling curves. This calibration of the imperfection amplitude of the pin-ended column leads to $w_0 = 11.5$ mm with an element mesh as used in the previous calculation. The residual stress pattern of Fig. 10 has been used with $\sigma_r = 0.3\sigma_y$ [2] instead of $\sigma_r = 0.5\sigma_y$ [7]. The corresponding load-deflection behaviour, line 2 in Fig. 11, is weak when compared with line 1.

An even weaker load-deflection behaviour, line 3 in Fig. 11, is found when the amplitude of the parabolic geometrical imperfection is calibrated, neglecting the influence of residual stresses. The equivalent geometrical imperfection so obtained, which includes the influence of residual stresses, is $w_0 = 14.3$ mm. The equivalent geometrical imperfection according to Eurocode No. 3 [8] is $w_0 = 12.7$ mm which would lead to an overestimation of the maximum strength of the column of Fig. 8.

Use of the imperfections prescribed [7, 8] in a geometrical and material non-linear analysis does not lead to an exact prediction of the maximum strength of centrally loaded pin-ended columns resulting from the ECCS buckling curves. Generally, for a numerical prediction of the maximum strength using a geometrical and material non-linear analysis, the imperfections of [7,8] can be used. However, if interaction formulae for beam-columns in non-sway frames are verified, imperfections of columns should be calibrated to the maximum strength of pin-ended columns according to buckling curves.

3.2 *Centrally loaded restrained column*

Besides residual stresses and geometrical imperfections, a third influence on the maximum strength of centrally loaded steel columns is also very important: end-restraints [6]. In [22] two methods to take account of end-restraints have been compared:

- use of the elastic effective length;
- use of the effective length, based on buckling curves for end-restrained columns.

It has been concluded that the method, using the elastic effective length together with multiple column curves for pin-ended columns, leads to safe estimations for the maxi-

mum strength of end-restrained, centrally loaded columns in non-sway frames if the restraints are strong enough to provide sufficient stiffness up to column collapse. This method, which is most suitable for use in building codes at the moment, has been adopted in Eurocode No. 3 [8].

The example in Fig. 12 [22] supports this conclusion. The centrally loaded column of Fig. 12a is an IPE80 column restrained at both ends by rotational springs with the same moment-rotation characteristic. Residual stresses ($\sigma_r = 0.3\sigma_y$) have been taken into account (Fig. 10) and the geometrical imperfection $w_0 = 5.25$ mm has been calibrated: the pin-ended column ($k = 0$) attains collapse at the maximum strength resulting from the ECCS buckling curves. The number of integration points and elements is the same as previously mentioned. In Fig. 12b, three values for the maximum strength of this restrained column are shown. The values F_1 and F_2 have been calculated taking geometrical and material non-linearity into account. The value F_3 has been calculated using the elastic effective length and the ECCS buckling curve a. The moment-rotation characteristics 1 and 2 of Fig. 12c have been used to calculate F_1 and F_2 respectively.

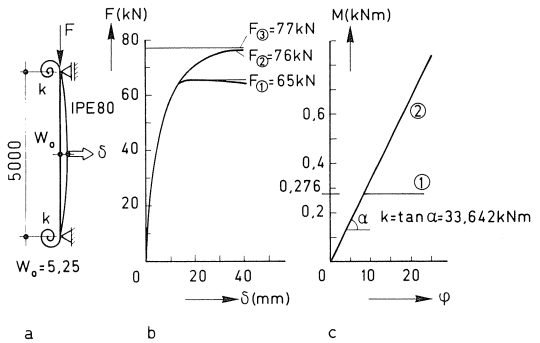

Fig. 12. Centrally loaded restrained steel column [22].

Moment-rotation characteristic 1 almost represents the strong axis connection moment-rotation data given in [23,25]. Moment-rotation characteristic 2 represents a linear spring. If the spring is strong enough up to column collapse (moment-rotation characteristic 2), the maximum strength based on the elastic effective length and the ECCS buckling curves is predicted very well.

3.3 *Non-sway frames*

Columns in non-sway frames can be checked using interaction formulae like for example equation (11), which shows the interaction formula as given in [8].

$$\frac{N}{\chi N_p} + \frac{1}{1 - \frac{N}{\chi N_p}(\chi\bar{\lambda})^2} \frac{\beta M}{M_p} \leqslant 1 \tag{11}$$

The reduction coefficient χ is determined using the multiple column curves of Fig. 7 and the slenderness parameter $\bar{\lambda}$. However, this slenderness parameter depends on the buckling length of the column considered. Although buckling curves have been derived for pin-ended columns, where the buckling length is equal to the length of the column, the elastic effective length which is smaller than the length of a column in a non-sway frame, is generally used as buckling length in interaction formulae.

The example of Fig. 13 supports the use of the elastic effective length in interaction formulae. The maximum strength of a column in the non-sway frame of Fig. 13 is esti-

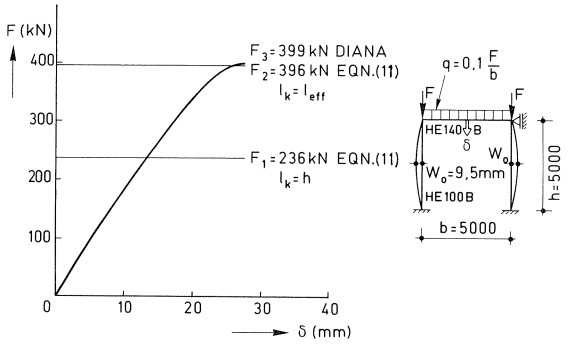

Fig. 13. Non-sway frame.

mated using equation (11). The normal compressive force N and the bending moment M are expressed in F using a linear elastic calculation. The maximum strength $F_1 = 236$ kN is solved from equation (11) using the length of the column as buckling length. If the elastic effective length is used as buckling length, $F_2 = 396$ kN is found as an estimation of the maximum column strength. If these values are compared with the maximum strength resulting from a geometrical and material non-linear analysis, $F_3 = 399$ kN, use of the column length turns out to be conservative and use of the elastic effective length in the interaction formula of equation (11) predicts the maximum strength very well.

The second non-sway frame to be considered is shown in Fig. 14a [21]. As explained in [24,26], for 'strong beam, weak column designs' a change of sign of the bending moment at the top of the columns can be observed. Fig. 14b shows the bending moments in the beam according to a linear elastic analysis compared with the bending moments in the beam at collapse, according to a geometrical and material non-linear

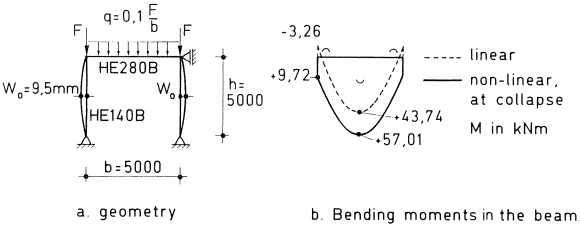

Fig. 14. Non-sway frame: change of sign of bending moment at the top of the column.

analysis. Indeed, the bending moment at the top of the column changes sign. The columns are restrained by the beam. In [16,27] the problem of change of sign of the bending moment at the top of the columns of a non-sway frame has been treated also. In [16] it is stated that the effective length method for the stability check of non-sway frames can be carried out without caring about the change of sign of the bending moment at the top of the column. In [27] concern is expressed on the use of the effective length concept together with a linear elastic static analysis and it is proposed to use a non-linear analysis always, to overcome the problems concerning the change of sign of the bending moment at the top of the column. However, according to [19,20,21] use of the elastic effective length as buckling length in interaction formulae, leads to safe estimations for the maximum strength of columns in non-sway frames, if the beams are strong enough and column collapse characterizes the frame behaviour. Therefore, the beam must be checked taking the change of sign of the bending moment into account. In [19,20,21] a design method for beams in non-sway frames is suggested, taking change of sign of the bending moment at the top of the columns into account. The connection between column and beam also has to be designed for a positive bending moment.

The geometrical and material non-linear analyses have been carried out using ten elements for each column and beam. Again 85 integration points per element have been used. Residual stresses ($\sigma_r = 0.3\sigma_y$) have been taken into account (Fig. 10) and the geometrical imperfection w_0 has been calibrated as described before. The previous two examples of centrally loaded columns have been analysed in a displacement-controlled way. This is impossible for the non-sway frames of Figs. 13 and 14 which have been analysed in a load-controlled way. Of course it is possible to make use of symmetry for the centrally loaded columns as well as for the non-sway frames discussed here.

3.4 *Sway frame*

If the sway frame of Fig. 15a is analysed taking geometrical and material non-linearity into account, imperfections have to be assumed. Here, the equivalent nominal load according to [8] has been used resulting in a total horizontal force $0.06F$ at the top of the left column, which consists of a real horizontal force $0.05F$ and an equivalent nominal load $0.01F$, accounting for geometrical imperfections and residual stresses. Again ten elements for each column and beam have been used as well as 85 integration points per element. The method proposed by Riks [17] and Wempner [28] has been used to study post-critical behaviour of this sway frame. Now, a limit point can be passed under load-

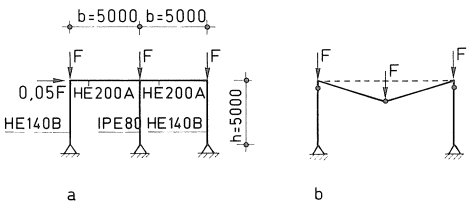

Fig. 15. Sway frame.

control way by help of the arc-length procedure. This sway frame cannot be analysed in a displacement controlled way since the points of application of the loads change relative to each other during loading. In Fig. 16, load-displacement curves are shown for:

- the horizontal displacement at the top of the right column δ_1;
- the horizontal displacement at mid-height of the centre column δ_2;
- the vertical displacement at the top of the centre column δ_3.

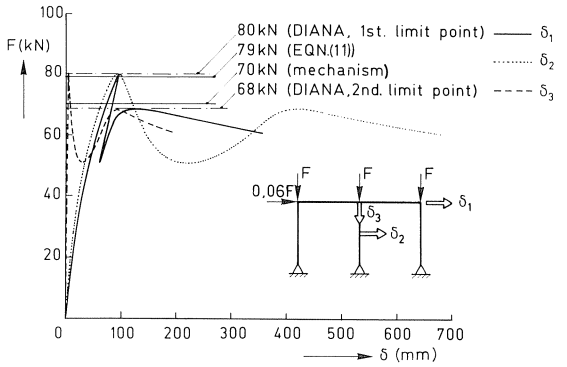

Fig. 16. Load-displacement curves of the sway frame.

The centre column is weak when compared with the left and right column. At $F=80$ kN the centre column collapses: the first limit point is reached. With decreasing load, the horizontal displacement at the top of the right column decreases: the frame sways back elastically. However, the horizontal displacement at mid-height and the vertical displacement at the top of the centre column still increase: the centre column has collapsed. The load decreases until this vertical displacement is so large that the two beams behave like one long beam which builds up resistance. At $F=51$ kN the load begins to increase until at $F=68$ kN a beam-mechanism is formed. At this moment the second limit point is reached. In Fig. 17 several subsequent deformed situations of the sway frame of Fig. 15a are shown.

The two limit points can be estimated analytically. The first limit point is determined

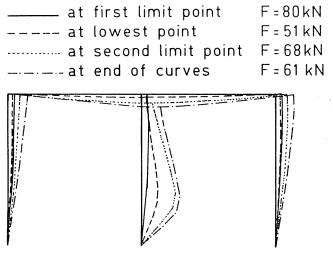

Fig. 17. Four subsequent deformed situations of the sway frame.

by collapse of the weak centre column. Use of equation (11), together with the multiple column curves for pin-ended columns and with the elastic effective length as buckling length, results in $F = 79$ kN as estimation for the maximum strength of the centre column. The second limit point is determined by a beam-mechanism as shown in Fig. 15b. The plastic moment capacities of the columns are influenced by the axial forces. When the reduced plastic moment capacities according to [8] are used, the collapse load of the beam-mechanism is $F = 70$ kN. The estimations of the two limit points are shown as horizontal lines in Fig. 16. These lines agree very well when compared with the numerically determined limit points.

The results of the calculations for the sway frame of Fig. 15a support the idea that use of the elastic effective length together with multiple column curves for pin-ended columns, leads to safe estimations for the maximum strength of beam-columns in sway frames.

Advanced solution procedures for non-linear structural behaviour enable the study of post-critical behaviour of frames. Alternative load-carrying paths can be found and post-critical strength can be determined.

4 Applications under fire conditions

The strength of steel structures at elevated temperatures is also influenced by the change of Young's modulus and the yield stress with increasing temperature. Therefore, the constitutive relation has been extended with temperature dependent material properties.

Usually for steel structures at elevated temperatures not the maximum strength of the structure but the critical temperature is relevant. This temperature is defined as the maximum steel temperature at failure. In fire tests structures are usually loaded up to the characteristic load.

To simulate an experiment and to verify the constitutive relation, not only the critical temperature but also the deformations at several points of the structure as function of the temperature have to be measured in the experiment. Besides the material behaviour other factors which can influence the deformation behaviour and critical temperature are: temperature variation along the axis of the column, small degree of unintended rotational restraint or unavoidable eccentricity of the load [31]. In Germany several experiments have been carried out where the deformations as function of temperature are measured. Two experiments are discussed here: a pin-ended beam-column and a non-sway frame [11].

In the calculations performed an elasto-(perfectly)plastic stress-strain relation is used in which Young's modulus and the yield stress change with increasing temperature, as shown in Fig. 18. The stress-strain relation is modelled with the Von Mises yield function and Hooke's law for the elastic stage. Unloading takes place elastically according to Young's modulus at the present temperature.

The difference between the stress-strain relations for the temperatures 200 °C and 300 °C in Fig. 18 is a result of the thermo-activated flow (transient strain) of steel under

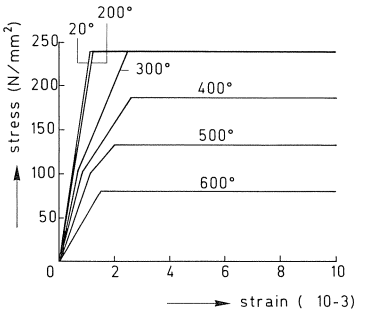

Fig. 18. Stress-strain relationships used for steel at elevated temperatures.

high stresses [11, 30]. The thermo-activated flow depends on the temperature increment and the stress level and has been incorporated in the constitutive relation as a transient strain [11]. Residual stresses ($\sigma_r = 0.3\sigma_r$) have been taken into account according to figure 10 and the geometrical imperfection has been calibrated at room temperature as previously described. In the material model the ratio between hardening and initial yield stress for the stress-strain relation of the flange, when residual stresses are taken into account, does not change. So the residual stresses are partly anealed at the critical temperature.

4.1 *Beam-column*

Since the out of plane deflection of the column remains small, the column is idealized with ten two-dimensional beam-column elements in which geometrical and material non-linearity has been taken into account. Each element has been divided in 3 sections and for each section 17 integration points have been used. In the computations the temperature varies with time after the load has been applied but is constant over the cross-section and along the axis. The experimental results [13] and the calculated results are shown in Fig. 19. The calculated deformation behaviour shows good resemblance to the experimental deformation behaviour. The differences in axial deformations between

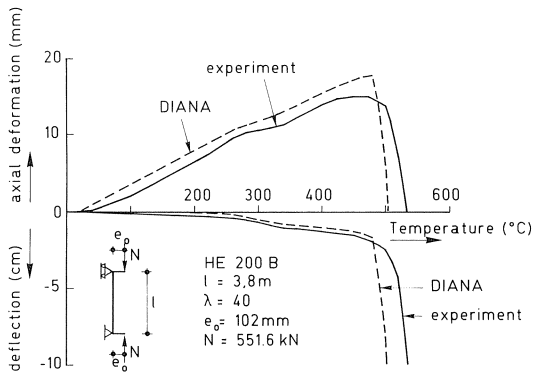

Fig. 19. Measured and calculated deformations of the column under fire conditions.

the computations and the experiment can be partly explained by the temperature variation along the column axis in the experiment which does not exist in the numerical analysis.

The increasing deformation of the column around 300 °C can be described well with the thermo-activated flow. Still, this phenomenon is point of discussion and will be the subject of further study. The estimation of the critical temperature is good. Comparing the temperatures at which the axial deformation is zero again, a 35 °C lower critical temperature is calculated than experimentally observed.

Because of the high eccentricity of the load for this beam-column, the value of the initial geometrical imperfection will not affect the critical temperature significantly.

Experiments carried out at other institutes [15] have also been analysed numerically with comparable results for the deformation behaviour. The difference between the constitutive relation given in [9,29] and the one of Fig. 18 is a subject for further research.

4.2 *Non-sway frame*

In Germany full-sized steel frames have been tested under fire conditions [14]. During the experiment deformations at several points have been measured. The out of plane deformation of the column remains very small so the frame can be idealized with two-dimensional beam-column elements. For the column and the beam in the non-sway frame ten elements each and 3 sections per element with 17 integration points per section have been used.

The frame consists of HE240B sections with a measured yield stress of 318.7 N/mm^2. The column is loaded by a central normal force of 686 kN and the beam is loaded with 25 kN/m (Fig. 20). The beam is covered on three sides and the column on all four sides

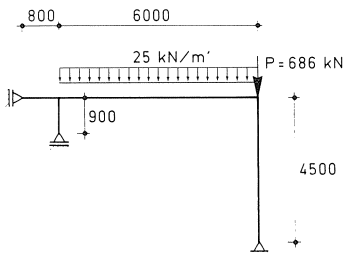

Fig. 20. Geometry of the non-sway frame under fire conditions.

with Vermitecta-plates which are 20 mm thick. In the computations, a linear temperature distribution over the cross-section of the beam is used [11] and in the column the temperature at the sections is uniformly distributed in conformity with the measured temperatures.

During the experiment, the axial deformation of beam and column, the deflection of the beam at mid-height, the in-plane deformation of the column at mid-span and the horizontal support reaction have been measured and are shown in the right half of Fig.

21 as a function of temperature. After the first computations, the experimental results were in doubt, because the measured temperatures were much too low when compared with the calculated ones. Indeed, it was ascertained that the temperatures had not been measured correctly. Since other information is not available, the calculated deformations are presented but cannot be compared quantitatively with the experimental results.

The critical temperature according to the European recommendations [9] for the fire safety of steel structures is 550 °C for the non-sway frame. This value is, as can be expected when comparing codes with experiments, on the safe side when compared to the calculated value 600 °C.

The computed deformations as a function of the temperature are shown in the left half of Fig. 21. It can be clearly seen that the global deformation behaviour is the same as registered in the experiment, e.g. the change of the horizontal force from compression to tension at the end of the experiment. Strain reversal in the column occurs and it

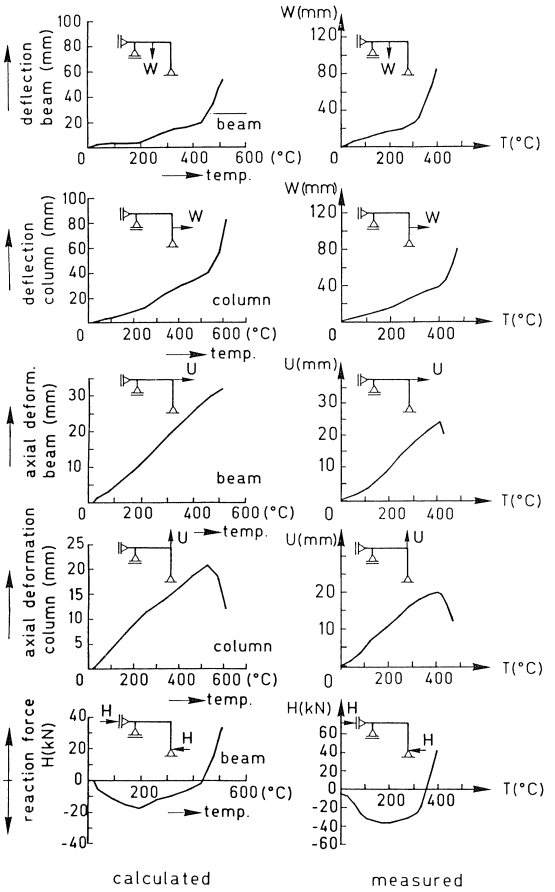

Fig. 21. Measured and calculated deformations of the non-sway frame under fire conditions. The highest temperatures occurring in the beam and the column have been plotted.

is assumed that unloading takes place according to the elastic stiffness at the present temperature.

5 Summary and conclusions

It has been shown in several examples that steel column and frame stability analyses using finite element techniques contribute to better understanding of the behaviour of these structures. Finite element techniques are powerful means to provide background information for developing design codes. The examples presented in this paper support the following conclusions.

- If interaction formulae for beam-columns in non-sway frames are verified, imperfections should be calibrated when non-sway frames are analysed, taking geometrical and material non-linearity into account. The amplitude of the parabolic imperfection has to be determined so that a pin-ended centrally loaded column with the same length as the column in the braced frame attains collapse at the maximum strength resulting from buckling curves.
- Use of the elastic effective length in interaction formulae together with multiple column curves for pin-ended columns, leads to safe estimations for the maximum strength of beam-columns in sway and non-sway frames.
  However, the restraining beams and the connections between beams and columns must be strong enough to provide sufficient stiffness up to column collapse.
  It is necessary to know the bending moment distribution at column collapse of the restraining beams in order to design the beams and the connections between beams and columns safely.
- Alternative load-carrying paths can be found and post-critical strength can be determined when advanced solution procedures for non-linear structural behaviour are used.
- The finite element calculations of the column and non-sway frame under fire conditions show good agreement with the experimental findings. The behaviour of steel structures at elevated temperatures can be simulated and also the critical temperature is well estimated. To verify constitutive relationships, it is necessary to measure the deformations of structures under fire conditions. Calibrated constitutive relations make it possible to analyse structures which cannot be experimentally investigated in the existing furnaces.

With the elements and constitutive relationships employed, which are verified by experiments, it is possible to analyse the deformation behaviour and the maximum strength of steel columns and frames at room temperatures and elavated temperatures.

6 Acknowledgement

The authors wish to express their thanks to ir. F. S. K. Bijlaard, ir. G. M. A. Kusters and ir. L. Twilt for the fruitful discussions that contributed to this paper.

7 Notation

a	displacement field
A	cross-sectional area
b	width
C	combination matrix
D_{nn}	matrix coefficients
e	linear contribution to strain
e_0	eccentricity
E	Young's modulus
F	load
h	height
H	hardening parameter
I	moment of inertia
k	rotational spring stiffness
K	stiffness matrix
K_L^{NL}	initial displacement matrix
K_σ^{NL}	initial stress matrix
l	length
M	moment
M_p	plastic moment capacity
N	normal force
N_E	Euler buckling load
N_p	squash load
P	external nodal force vector
P_ε	external generalized nodal force vector
q	uniformly distributed load
S_ε	generalized stiffness matrix
S_ε^N	non-linear generalized stiffness matrix
S_{nn}	matrix coefficients
u	displacement field in the direction of the element axis
u_k	axial degree of freedom at the middle of the element axis
v	nodal displacements
v_ε	generalized nodal displacements
V	shear force
V_0	volume
w	displacement field perpendicular to the element axis
w_0	imperfection amplitude
x	coordinate along the element axis
y	distance from layer to element axis
y_z	shift of centroidal axis from element axis
β	equivalent moment factor
δ	displacement

Δ	increment
Δl	generalized elongation of an element
ε	strain
ε_c	creep strain
ε_e	elastic strain
ε_g	average strain at element axis
$\bar{\varepsilon}_g$	average strain at centroidal axis
ε_p	plastic strain
ε_Θ	thermal strain
η	non-linear contribution to strain
Θ	temperature
$\varkappa$	curvature
λ	slenderness
$\bar{\lambda}$	slenderness parameter
σ	stress
σ^e	test stress
σ_k	buckling stress
σ_r	residual stress
σ_y	yield stress
φ	nodal rotation
χ	buckling coefficient
ψ_i, ψ_j	generalized nodal rotations at nodes *i* and *j* respectively
Ψ	relative coordinate

8 References

1. Bathe, K. J., Finite Element Procedures in Engineering Analysis, Prentice Hall, Inc., Englewood Cliffs, New Jersey 07632, 1982.
2. Beedle, L. S. and Tall, L., Basic Column Strength, Journal of the Structural Division, Proc. ASCE, Vol. 86 (1960), no. ST7, pp. 138-173.
3. Beer, H. and Schulz, G., Theoretical Basis of the European Column Curves, Construction Métallique, Vol. 7 (1970), pp. 37-57.
4. Blaauwendraad, J., Realistic Analysis of Reinforced Concrete Framed Structeres. HERON, Vol. 18 (1972), no. 4.
5. Borst, R. de, Application of Advanced Solution Techniques to Concrete Cracking and Non-associated Plasticity, Numerical Methods for Non-linear Problems, Vol. 2, edited by C. Taylor, E. Hinton, D. R. J. Owen, Pineridge Press, Swansea, 1984.
6. Chen, W.F., End-Restraint and Column Stability, ASCE, Journal of the Structural Division, Vol. 106 (1960), pp. 2279-2295.
7. ECCS-Technical Committee 8, Structural Stability Technical Working Group 8, Systems, Ultimate Limit State Calculations of Sway Frames with Rigid Joints, ECCS-CECM-EKS, Publication No. 33, first edition, 1984.
8. Eurocode No. 3, Common Unified Rules for Steel Structures, report EUR 8849 DE, EN, FR, ECSC-EEG-EAEC, Brussels-Luxembourg, 1984.
9. European Recommendations for the Fire Safety of Steel Structures, ECCS, Technical Committee 3, Fire Safety of Steel Structures.

10. FOEKEN, R.J. VAN, Evaluation of the Thermo-Elasto-Plastic-Creep Material Model in Combination with Cracking, Report no. BI-84-63, TNO Institute for Building Materials and Structures, Rijswijk, The Netherlands, December 1984.
11. FOEKEN, R.J. VAN, Numerical Analyses of Steel and Concrete Structures under Fire Conditions. Report no. BI-85-23, TNO Institute for Building Materials and Structures, Rijswijk, The Netherlands, March 1985.
12. FOEKEN, R.J. VAN, Numerical Analyses of Reinforced Concrete Structures at High Temperatures including Cracking Plasticity and Creep, Paper presented at the Fourth International Conference on Numerical Methods in Thermal Problems, July 15th-18th, Swansea, 1985.
13. HOFFEND, F., Brandverhalten von Stahlstützen bei ausmittiger Lasteinleitung, Dehnbehinderung oder teilweiser Bekleidung, Sonderforschungsbereich 148, Brandverhalten von Bauteilen-, Arbeitsbericht 1978-1980, Teil 1, T.U. Braunschweig, Juni 1980.
14. HOFFEND, F., Brandversuche an Stahlrahmen, Versuchsergebnisse, deren Analyse und rechnerische Vergleiche, Sonderforschungsbereich 148, Brandverhalten von Bauteilen-, Arbeitsbericht 1978-1980, Teil 1, T.U. Braunschweig, Juni 1980.
15. JANSS, J. and MINNE, R., Buckling of Steel Columns in Fire Conditions, Fire Safety Journal, 4 (1981/82), pp. 227-235.
16. KINDMANN, R., Zum Tragverhalten ebener Rahmen aus Baustahl, Festschrift Roik, Technischwissenschaftliche Mitteilungen, Institut für Konstruktiven Ingenieurbau, Ruhr-Universität Bochum, Mitteilung Nr. 84-3, September 1984, pp. 200-214.
17. RIKS, E., An Incremental Approach to the Solution of Snapping and Buckling Problems, Int. J. Solids Structures, Vol. 15 (1979), pp. 529-551.
18. SFINTESCO, D., Experimental Basis of the European Column Curves, Construction Métallique, Vol. 7 (1970), pp. 5-12.
19. SNIJDER, H. H., BIJLAARD, F. S. K. and STARK, J. W. B., Use of the Elastic Effective Length for Stability Checks of Columns and Consequences for Checks on Beams in Braced Frames, Instability and Plastic Collapse of Steel Structures, Proc. of the Michael R. Horne Conference, Edited by L. J. Morris, London, Granada, 1983, pp. 152-163.
20. SNIJDER, H. H., BIJLAARD, F. S. K. and STARK, J. W. B., Strength Requirement for Beams in Braced Frames in Relation to Column Stability, Third International Colloquium, Stability of Metal Structures, Final Report, Paris, 1983, pp. 247-251.
21. SNIJDER, H. H., BIJLAARD, F. S. K. and STARK, J. W. B., Design of Braced Frames using the Elastic Effective Length Method, Festschrift Roik, Technisch-wissenschaftliche Mitteilungen, Institut für Konstruktiven Ingenieurbau, Ruhr-Universität Bochum, Mitteilung Nr. 84-3, September 1984, pp. 316-332.
22. SNIJDER, H. H. and BIJLAARD, F. S. K., The Influence of End-Restraints on the Maximum Strength of Centrically Loaded Columns in Braced Frames, J. Construct. Steel Research, Vol. 5 (1985), pp. 137-147.
23. SUGIMOTO, H. and CHEN, W.F., Small End-Restraint Effect on Strength of H-Columns, ASCE, Journal of the Structural Division, Vol. 108 (1982), pp. 661-680.
24. VINNAKOTA, S., Design of Columns in Planar Frames - A few Comments, Proc. of the National Conference on 'Tall Buildings' held at New Delhi, 1973.
25. VINNAKOTA, S., Planar Strength of Restrained Beam Columns, ASCE, Journal of the Structural Division, Vol. 108 (1982), pp. 2496-2516.
26. VINNAKOTA, S., Design of Columns as Part of Frames - Some Remarks, Paper submitted to TG3: SSRC, 1983.
27. VOGEL, U., Gedanken zum Sinn und zur Zuverlässigkeit des Tragsicherheitsnachweises am Ersatzstab bei Stabsystemen, Festschrift Roik, Technisch-wissenschaftliche Mitteilungen, Institut für Konstruktiven Ingenieurbau, Ruhr-Universität Bochum, Mitteilung Nr. 84-3, September 1984, pp. 333-346.
28. WEMPNER, G.A., Discrete Approximations related to Non-linear Theories of Solids, Int. J. Solids Structures, Vol. 7 (1971), p. 1581.
29. WITTEVEEN, J. and TWILT, L., Behaviour of Steel Columns under Fire Conditions, Int. Coll. on Column Strength, Paris, 1972, Proc. IABSE, Vol. 23, Zürich, 1975.

30. WITTEVEEN, J., TWILT, L. and BIJLAARD, F. S. K., The Stability of Braced and Unbraced Frames at Elevated Temperatures, 2nd Int. Coll. on the Stability of Steel Structures, Liège, 1977, Preliminary Report.
31. WITTEVEEN, J. and TWILT, L., A Critical View on the Results of Standard Fire Resistance Tests on Steel Columns. Fire Safety Journal, 4 (1981/82), pp. 259–270.

APPENDIX A

Derivation of the linear stiffness matrix

To determine the relation between the external loads and the deformation field of the beam-column element the principle of virtual work which describes equilibrium between internal and external forces is used within a total Lagrangian description [1]:

$$\int_{V_0} \partial\varepsilon^{\mathrm{T}}\sigma \, \mathrm{d}V = P\partial a \tag{A.1}$$

where a is the displacement field, σ the stress field, ε the strain field and P is the external force vector.

In non-linear analysis the load is applied in small increments. Therefore, equation (A.1) must be incrementally formulated. Let 0 refer to the beginning of the increment. Substituting $\sigma = \sigma^0 + \Delta\sigma$ and $P = P^0 + \Delta P$ in equation (A.1) leads to:

$$\int_{V_0} \partial\varepsilon^{\mathrm{T}} \Delta\sigma \, \mathrm{d}V = P\partial a - \int_{V_0} \partial\varepsilon^{\mathrm{T}}\sigma^0 = \Delta P \partial a \tag{A.2}$$

The right hand side of equation (A.2) corresponds to the incremental external load.

Integration of equation (A.2) over the cross-section of the element and expressed in average strain and curvature gives the following formulation for the beam-column element:

$$\int_0^l \partial \begin{bmatrix} \Delta\varepsilon_{\mathrm{g}} & \Delta\varkappa \end{bmatrix} \begin{bmatrix} D_{11} & D_{12} \\ D_{21} & D_{22} \end{bmatrix} \begin{bmatrix} \Delta\varepsilon_{\mathrm{g}} \\ \Delta\varkappa \end{bmatrix} \mathrm{d}l = \Delta P \partial a \tag{A.3}$$

where:

$$D_{11} = \int_A E \, \mathrm{d}A$$

$$D_{21} = \int_A yE \, \mathrm{d}A$$

$$D_{12} = D_{21}$$

$$D_{22} = \int_A y^2 E \, \mathrm{d}A$$

For stable equilibrium, equation (A.2) must hold for any virtual displacement. Equation (A.2) expressed in generalized incremental displacements for a load step, results in equation (A.4) by substituting equations (1), (2) and (3):

$$\begin{bmatrix} S_{11} & S_{12} & S_{13} & S_{14} \\ S_{21} & S_{22} & S_{23} & S_{24} \\ S_{31} & S_{32} & S_{33} & S_{34} \\ S_{41} & S_{42} & S_{43} & S_{44} \end{bmatrix} \begin{bmatrix} \Delta u_{\mathrm{k}} \\ \Delta\Delta l \\ \Delta\psi_{\mathrm{i}} \\ \Delta\psi_{\mathrm{j}} \end{bmatrix} = \begin{bmatrix} 0 \\ \Delta N \\ \Delta M_{\mathrm{i}} \\ \Delta M_{\mathrm{j}} \end{bmatrix} \tag{A.4}$$

The terms S_{nn} with $\Psi = x/l$ are integrals of the form [4]:

$$S_{11} = \frac{1}{l}\int_0^1 (4-8\Psi)^2 D_{11}\,\mathrm{d}\Psi$$

$$S_{21} = S_{12} = \frac{1}{l}\int_0^1 (4-8\Psi) D_{11}\,\mathrm{d}\Psi$$

$$S_{31} = S_{13} = \frac{1}{l}\int_0^1 (4-8\Psi)(4-6\Psi) D_{12}\,\mathrm{d}\Psi$$

$$S_{41} = S_{14} = \frac{1}{l}\int_0^1 (4-8\Psi)(2-6\Psi) D_{12}\,\mathrm{d}\Psi$$

$$S_{22} = \frac{1}{l}\int_0^1 D_{11}\,\mathrm{d}\Psi$$

$$S_{32} = S_{23} = \frac{1}{l}\int_0^1 (4-6\Psi) D_{12}\,\mathrm{d}\Psi$$

$$S_{42} = S_{24} = \frac{1}{l}\int_0^1 (2-6\Psi) D_{12}\,\mathrm{d}\Psi$$

$$S_{33} = \frac{1}{l}\int_0^1 (4-6\Psi)^2 D_{22}\,\mathrm{d}\Psi$$

$$S_{43} = S_{34} = \frac{1}{l}\int_0^1 (2-6\Psi)(4-6\Psi) D_{22}\,\mathrm{d}\Psi$$

$$S_{44} = \frac{1}{l}\int_0^1 (2-6\Psi)^2 D_{22}\,\mathrm{d}\Psi$$

Equation (A.4) can be written in a more compact way:

$$\begin{bmatrix} S_{uu} & S_{u\varepsilon} \\ S_{\varepsilon u} & S_{\varepsilon\varepsilon} \end{bmatrix} \begin{bmatrix} \Delta u_k \\ \Delta v_\varepsilon \end{bmatrix} = \begin{bmatrix} 0 \\ \Delta P_\varepsilon \end{bmatrix} \tag{A.5}$$

Since the external load on the node in the middle of the element is zero, equation (A.5) can be reduced to:

$$[S_{\varepsilon\varepsilon} - S_{\varepsilon u} S_{uu}^{-1} S_{u\varepsilon}]\,\Delta v_\varepsilon = S_\varepsilon\,\Delta v_\varepsilon = \Delta P_\varepsilon \tag{A.6}$$

The relationships between the generalized displacements and forces and the nodal displacements and forces are given by:

$$v_\varepsilon = Cv \qquad P = C^T P_\varepsilon \tag{A.7}$$

with:

$$C=\begin{bmatrix} -1 & 0 & 0 & 1 & 0 & 0 \\ 0 & \frac{1}{l} & 1 & 0 & \frac{-1}{l} & 0 \\ 0 & \frac{1}{l} & 0 & 0 & \frac{-1}{l} & 1 \end{bmatrix}$$

Equations (A.6) and (A.7) can be combined to find the final incremental relationship between the external loads and the deformation field for the beam-column element:

$$C^{\mathrm{T}} S_C \, \Delta v = K \, \Delta v = \Delta P \tag{A.8}$$

APPENDIX B

Derivation of the geometrical non-linear stiffness matrices

In case of large displacements but small strains (equation (4)) a non-linear contribution to the strain, $\eta = \frac{1}{2}(\mathrm{d}w/\mathrm{d}x)^2$, has to be taken into account. This leads to an extra term in the incremental virtual work equation (A.2):

$$\int_{V_0} \partial\varepsilon^{\mathrm{T}} \Delta\sigma \, \mathrm{d}V + \int_{V_0} \partial\eta^{\mathrm{T}} \sigma^0 \, \mathrm{d}V = P\partial a - \int_{V_0} \partial e^{\mathrm{T}} \sigma^0 = \Delta P \partial a \tag{B.1}$$

The non-linear term

$$\int_{V_0} \partial\eta^{\mathrm{T}} \sigma^0 \, \mathrm{d}V$$

consists of an initial stress matrix, K_σ^{NL} and an initial displacement matrix, $K_{\mathrm{L}}^{\mathrm{NL}}$. The final incremental relationship between the external loads and the deformation field, including large displacements, is an extension of equation (A.8)

$$(C^{\mathrm{T}} S_\varepsilon C + C^{\mathrm{T}} S_\varepsilon^{\mathrm{N}} C + K_{\mathrm{L}}^{\mathrm{NL}}) \Delta v = (K + K_\sigma^{\mathrm{NL}} + K_{\mathrm{L}}^{\mathrm{NL}}) \Delta v = \Delta P \tag{B.2}$$

with:

$$S_\varepsilon^{\mathrm{N}} = \begin{bmatrix} 0 & 0 & 0 \\ 0 & \frac{2}{15} Nl & \frac{-1}{30} Nl \\ 0 & \frac{-1}{30} Nl & \frac{2}{15} Nl \end{bmatrix} \tag{B.3}$$

$$K_\sigma^{\mathrm{NL}} = \begin{bmatrix} 0 & 0 & 0 & 0 & 0 & 0 \\ 0 & \frac{N}{5l} & \frac{1}{10} N & 0 & \frac{-N}{5l} & \frac{1}{10} N \\ 0 & \frac{1}{10} N & \frac{2}{15} Nl & 0 & \frac{-1}{10} N & \frac{-1}{30} Nl \\ 0 & 0 & 0 & 0 & 0 & 0 \\ 0 & \frac{-N}{5l} & \frac{-1}{10} N & 0 & \frac{N}{5l} & \frac{-1}{10} N \\ 0 & \frac{1}{10} N & \frac{-1}{30} Nl & 0 & \frac{-1}{10} N & \frac{2}{15} Nl \end{bmatrix} \tag{B.4}$$

$$K_{\mathrm{L}}^{\mathrm{NL}} = \begin{bmatrix} 0 & 0 & 0 & 0 & 0 & 0 \\ 0 & \frac{N}{l} & 0 & 0 & \frac{-N}{l} & 0 \\ 0 & 0 & 0 & 0 & 0 & 0 \\ 0 & 0 & 0 & 0 & 0 & 0 \\ 0 & \frac{-N}{l} & 0 & 0 & \frac{N}{l} & 0 \\ 0 & 0 & 0 & 0 & 0 & 0 \end{bmatrix} \tag{B.5}$$

The initial stress matrix accounts for the second order generalized deformations caused by the normal force and the initial displacement matrix is a correction for additional reactions caused by the normal force due to an inclination of the member.